Journal of Physics: Conference Series **135** (2008) 012055 doi:10.1088/1742-6596/135/1/012055

Total wavefield-based inversion in PML-truncated domains

J Kang[1] **and L F Kallivokas**[1,2]

[1] Department of Civil, Architectural and Environmental Engineering
[2] The Institute for Computational Engineering and Sciences
The University of Texas at Austin
1 University Station, C1748
Austin, TX 78712, USA

E-mail: jwkang@mail.utexas.edu, loukas@mail.utexas.edu

Abstract. We discuss a total wavefield-based inversion approach for the reconstruction of the material profile of heterogeneous semi-infinite domains, directly in the time domain, based on scant surficial measurements of the domain's response to prescribed wave illumination. Of particular interest is the ability to recover the in-depth profile of moduli/wave velocities typically associated with small-scale geotechnical site characterization applications. We address four key issues associated with the wavefield-based inversion: a) to limit the semi-infinite extent of the physical domain, a perfectly-matched-layer (PML) is introduced at truncation interfaces to render a finite computational domain; b) to account for the introduction of the PML, while retaining the second-order temporal character of the hyperbolic problem, we discuss a new mixed unsplit-field formulation for the coupled PML-regular-domain problem; c) to tackle the inversion, we adopt a PDE-constrained optimization framework that formally leads to a classic (time-dependent) KKT (Karush-Kuhn-Tucker) system; and d) to alleviate solution multiplicity, we discuss a first-order Tikhonov regularization scheme endowed with a regularization factor continuation algorithm. We report on one- and two-dimensional experiments that lead efficiently to the reconstruction of heterogeneous profiles involving both horizontal and inclined layers, as well as of inclusions within layered systems.

1. Introduction

We are concerned with the reconstruction of the material profile in a halfplane, when the host medium is probed with interrogating waves. The quintessential application is in geotechnical site characterization, but the problem is commonly encountered across various science and engineering disciplines. When the interrogated host is of infinite or semi-infinite extent, as is the case with geotechnical or geophysical applications, there is need to truncate the unbounded domain in order to arrive at a computationally finite region. To this end, many absorbing boundary schemes have been developed, both local [1], or non-local [2]. Such schemes have shown reasonable wave-absorption performance for boundaries with special geometry, for homogeneous or layered systems, but have, by and large, difficulties in the presence of inhomogeneities or anisotropy. In this context, the contemporary perfectly-matched-layer (PML) approach seems to give rise to a promising wave-absorbing condition, since it has been shown to absorb outgoing waves without generating reflections for all frequencies and angles of incidence [3, 4, 5], even when the medium is heterogeneous. Thus, in this work we favor PMLs, and discuss the casting

of both the forward and inverse problem over a finite computational domain using PMLs on the truncation boundary. Herein, a new mathematical formulation of mixed unsplit-field PMLs is developed for two-dimensional SH waves (corresponding one-dimensional equations are presented without derivation). We discuss a mixed finite element scheme for solving the developed PML equations directly in the time-domain.

To describe the inverse problem, we discuss a partial-differential-equation (PDE)-constrained optimization approach [7, 8] for recovering the spatial variation of the soil's shear wave velocity. We start with a misfit functional between measured and computed responses to a dynamic surface excitation, using full waveforms directly in the time-domain. Then a Lagrangian functional is constructed where the misfit is augmented through the weak imposition of the governing PDEs for the system comprising the regular-domain and PML. Following classical lines, we seek to reconstruct the profile by requiring that the first-order optimality conditions be satisfied. There result time-dependent state, adjoint, and time-independent control problems, which, upon discretization lead to a classic KKT (Karush-Kuhn-Tucker) system. Here, the state and adjoint problems are resolved by a mixed finite element method. We iteratively update the shear wave velocity profile by solving the KKT system via a reduced-space approach. We explore Total Variation (TV) and Tikhonov (TN) regularization schemes to narrow the feasibility space and alleviate difficulties with solution multiplicity typically associated with such inverse problems. We present the inverse formulation in two dimensions and report on one- and two-dimensional experiments that lead efficiently to the reconstruction of heterogeneous profiles involving both horizontal and inclined layers, as well as of inclusions within layered systems.

2. Forward PML formulation

In this section we discuss the modeling of transient SH waves within unbounded domains, using an unsplit-field PML approach as a truncation condition.

2.1. Mixed unsplit-field PML formulation in the time-domain

The SH wave motion is governed, in the frequency domain, by the following system of equations:

$$\nabla \cdot \hat{\boldsymbol{\sigma}} = -\omega^2 \rho \hat{u}, \qquad \hat{\boldsymbol{\sigma}} = 2\mu \hat{\boldsymbol{\epsilon}}, \qquad \hat{\boldsymbol{\epsilon}} = \frac{1}{2}\nabla \hat{u}, \tag{1}$$

in which u denotes anti-plane displacement and $\boldsymbol{\sigma} = [\sigma_{31} \ \sigma_{32}]^{\mathrm{T}}$ is a vector of shear stress components. To solve Eqs.(1) within a domain of semi-infinite extent, we truncate the domain, attach a PML on the truncation boundary of the now finite computational domain of interest, and enforce the attenuation of the outgoing waves within the PML. Figure 1a depicts the truncated computational domain surrounded by the PML.

Figure 1. (a) A PML-truncated semi-infinite domain in two dimensions; (b) conceptual configuration of material profile reconstruction in a PML-truncated semi-infinite domain

Wave attenuation within the PML is attained via complex coordinate stretching [3, 4, 5]. To this end, we introduce stretched coordinates $\tilde{x}_1$ and $\tilde{x}_2$ as:

$$\tilde{x}_j = \int_0^{x_j} \lambda_j(s)ds = \int_0^{x_j} \left[\left\{ 1 + f_j^e(s) \right\} - i\frac{f_j^p(s)}{a_0} \right] ds, \quad j = 1, 2, \tag{2}$$

where f_j^e and f_j^p are attenuation functions for evanescent and propagating waves, respectively, in each j direction ($j = 1, 2$). $a_0 (= kb)$ denotes dimensionless frequency, k is a wave number, and b is a characteristic length of the system. We rewrite Eqs.(1) based on the stretched coordinates and then apply the inverse Fourier transform to obtain the following system in the time-domain:

$$f_m\ddot{v} + \frac{c_s}{b}f_c\dot{v} + \frac{c_s^2}{b^2}f_k v - \nabla \cdot \left(\tilde{\mathbf{F}}^e\dot{\mathbf{s}} + \tilde{\mathbf{F}}^p\mathbf{s} \right) = 0, \tag{3a}$$

$$\mathbf{F}^e\ddot{\mathbf{s}} + \mathbf{F}^p\dot{\mathbf{s}} - c_s^2\nabla\dot{v} = 0, \tag{3b}$$

where f_m, f_c, and f_k denote PML attenuation functions in terms of f_j^e and f_j^p ($j = 1, 2$), while $\tilde{\mathbf{F}}^e$, $\tilde{\mathbf{F}}^p$, $\mathbf{F}^e$, and $\mathbf{F}^p$ define stretch tensors [3, 4]. $c_s (= \sqrt{\mu/\rho})$ denotes shear wave velocity, and $v (= \rho u)$ is an auxiliary displacement variable. In (3), we introduced the stress memory $\mathbf{s}$ defined as:

$$\mathbf{s}(\mathbf{x}, t) = \int_0^t \boldsymbol{\sigma}(\mathbf{x}, \tau)d\tau \quad , \qquad \mathbf{s} = [s_1 \quad s_2]^{\mathrm{T}}, \tag{4}$$

such that

$$\dot{\mathbf{s}}(\mathbf{x}, t) = \boldsymbol{\sigma}(\mathbf{x}, t), \qquad \ddot{\mathbf{s}}(\mathbf{x}, t) = \dot{\boldsymbol{\sigma}}(\mathbf{x}, t). \tag{5}$$

Equations (3) are the displacement(v)-stress memory($\mathbf{s}$) mixed equations governing the propagation of SH waves in the PML-truncated domain $\Omega = \Omega_{\text{regular}} \cup \Omega_{\text{PML}}$. In the one-dimensional case, the corresponding displacement(v)-stress(σ) equations are:

$$\frac{\partial^2 v}{\partial t^2} + \left(\frac{cf}{b} + \zeta \right) \frac{\partial v}{\partial t} + \zeta\frac{cf}{b}v - \frac{\partial \sigma}{\partial x} = 0, \tag{6a}$$

$$\frac{\partial \sigma}{\partial t} + \frac{cf}{b}\sigma - c^2\frac{\partial^2 v}{\partial x \partial t} = 0, \tag{6b}$$

in which $c (= \sqrt{E/\rho})$ is the compressional wave velocity, and ζ is a parameter describing material damping, and f is the one-dimensional attenuation function.

2.2. Mixed finite element implementation

The PML equations can be implemented using a mixed finite element method [6]. For Eqs.(3), the trial functions $v(\mathbf{x}, t)$, $s_1(\mathbf{x}, t)$, $s_2(\mathbf{x}, t)$, and the corresponding test functions $w(\mathbf{x})$, $p(\mathbf{x})$, $q(\mathbf{x})$ are spatially discretized as:

$$v(\mathbf{x}, t) \simeq \boldsymbol{\phi}(\mathbf{x})^{\mathrm{T}}\mathbf{v}(t), \quad s_1(\mathbf{x}, t) \simeq \boldsymbol{\psi}(\mathbf{x})^{\mathrm{T}}\mathbf{s}_1(t), \quad s_2(\mathbf{x}, t) \simeq \boldsymbol{\psi}(\mathbf{x})^{\mathrm{T}}\mathbf{s}_2(t), \tag{7}$$

$$w(\mathbf{x}) \simeq \mathbf{w}^{\mathrm{T}}\boldsymbol{\phi}(\mathbf{x}), \quad p(\mathbf{x}) \simeq \mathbf{p}^{\mathrm{T}}\boldsymbol{\psi}(\mathbf{x}), \quad q(\mathbf{x}) \simeq \mathbf{q}^{\mathrm{T}}\boldsymbol{\psi}(\mathbf{x}), \tag{8}$$

where $\boldsymbol{\phi}$ and $\boldsymbol{\psi}$ are vectors of approximants associated with nodal displacements $\mathbf{v} (= \rho\mathbf{u})$ and nodal stress memories $\mathbf{s}_1$ and $\mathbf{s}_2$, respectively. In the two-dimensional case, we opted for a linear approximant pair for both $\boldsymbol{\phi}$ and $\boldsymbol{\psi}$, which *numerically* has been seen to yield stable solutions. By contrast, in the one-dimensional case, stable solutions are obtained if $\boldsymbol{\phi}$ and $\boldsymbol{\psi}$ are piecewise linear and piecewise constant, respectively. As a numerical test of the forward problem implementation, Fig. 2 depicts snapshots of displacement u, and shear stresses σ_{31} and

σ_{32} due to a Ricker pulse with a central frequency $f_r = 15$Hz exerted on a portion of the surface ($-0.5\text{m} < x_1 < 0.5\text{m}$). It is seen that the waves are excellently absorbed at the regular- and PML-domain interfaces without reflections. The suggested mixed unsplit-field PML formulation has advantages over either the split-field PML, which typically entails more unknowns (the split fields) [5], or a displacement-based PML scheme, which requires non-linear temporal integration schemes [4].

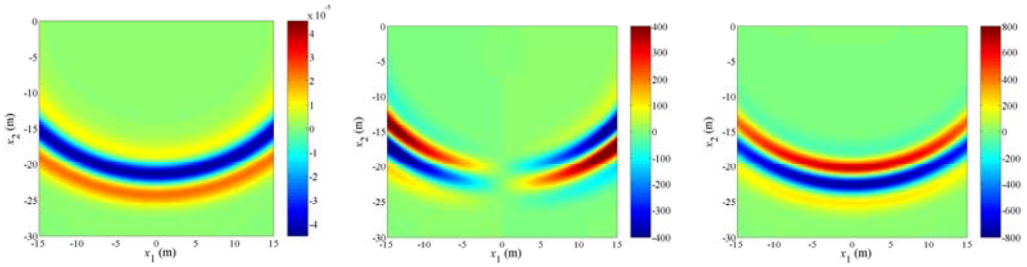

(a) (b) (c)

Figure 2. Snapshots of (a) u, (b) σ_{31}, and (c) σ_{32} for the surficial Ricker pulse load with characteristic frequency $f_r = 15$Hz

3. Inverse PML formulation using a PDE-constrained optimization

We discuss next the inverse PML formulation aimed at reconstructing the material profile using the newly developed PML scheme. Figure 1b depicts a two-dimensional semi-infinite domain occupied by a heterogeneous soil medium truncated by PMLs on its side and bottom edges. The goal is to recover the heterogeneous shear wave velocity profile (c_s) of Ω_{regular}.

3.1. Inverse misfit problem

Referring to Fig. 1, the inverse misfit problem for reconstructing the shear wave velocity profile (c_s) in the PML-truncated domain can be cast as follows:

$$\min \mathcal{F} := \frac{1}{2}\sum_{j=1}^{N_r}\int_0^T \int_{\Gamma_{\text{free}}} \left[v(\mathbf{x},t) - v_m(\mathbf{x},t)\right]^2 \delta\left(\mathbf{x}-\mathbf{x}_{mj}\right) d\Gamma_{\text{free}} dt \;+\; \mathcal{R}_{c_s}\left(c_s\right) \tag{9}$$

subject to the initial and boundary value problem (IBVP):

$$f_m\ddot{v} + \frac{c_s}{b} f_c \dot{v} + \frac{c_s^2}{b^2} f_k v - \nabla\cdot\left(\tilde{\mathbf{F}}^e\dot{\mathbf{s}} + \tilde{\mathbf{F}}^p\mathbf{s}\right) = 0, \quad \text{in } \Omega\times(0,T]\,, \tag{10a}$$

$$\mathbf{F}^e\ddot{\mathbf{s}} + \mathbf{F}^p\dot{\mathbf{s}} - c_s^2\nabla\dot{v} = 0, \quad \text{in } \Omega\times(0,T]\,, \tag{10b}$$

$$v(\mathbf{x},t) = 0 \quad \text{on } \Gamma_{\text{fixed}}\times[0,T], \tag{11a}$$

$$\dot{s}_2(\mathbf{x},t) = g(\mathbf{x},t) \quad \text{on } \Gamma_{\text{free}}\times[0,T], \tag{11b}$$

$$v(\mathbf{x},t) = 0 \quad \text{on } \Omega\times\{t=0\}\,, \tag{11c}$$

$$\dot{v}(\mathbf{x},t) = 0 \quad \text{on } \Omega\times\{t=0\}\,, \tag{11d}$$

$$\mathbf{s}(\mathbf{x},t) = 0 \quad \text{on } \Omega\times\{t=0\}\,, \tag{11e}$$

$$\dot{\mathbf{s}}(\mathbf{x},t) = 0 \quad \text{on } \Omega\times\{t=0\}\,. \tag{11f}$$

Here, N_r is the number of receivers on the surface, and $v_m(\mathbf{x}_{mj},t)$ is the measured displacement response at each receiver point ($\mathbf{x}_{mj}$) to dynamic surface excitation. We try to find the shear wave velocity profile (c_s) which minimizes the objective functional (9), subject to the governing PDEs (Eqs.(10b)), and boundary and initial conditions (Eqs.(11)).

3.2. Augmented Lagrangian functional

We recast the inverse problem (9)-(11) as an unconstrained optimization problem by defining an augmented Lagrangian functional $\mathcal{L}$ [7, 8]:

$$\begin{aligned}
&\mathcal{L}\left(v, s_1, s_2, \lambda_v, \lambda_{s_1}, \lambda_{s_2}, \lambda_B, \lambda_I, c_s\right) \\
&= \frac{1}{2}\sum_{j=1}^{N_r}\int_0^T\int_{\Gamma_{\text{free}}}\left[v(\mathbf{x},t)-v_m(\mathbf{x},t)\right]^2\delta\left(\mathbf{x}-\mathbf{x}_{mj}\right)d\Gamma_{\text{free}}dt + \frac{R_{c_s}}{2}\int_\Omega \nabla c_s\cdot\nabla c_s d\Omega \\
&+ \int_\Omega\int_0^T \lambda_v\left\{f_m\frac{\partial^2 v}{\partial t^2}+\frac{c_s}{b}f_c\frac{\partial v}{\partial t}+\frac{c_s^2}{b^2}f_k v-\nabla\cdot\left(\tilde{\mathbf{F}}^e\dot{\mathbf{s}}+\tilde{\mathbf{F}}^p\mathbf{s}\right)\right\}dtd\Omega \\
&+ \int_\Omega\int_0^T \lambda_{s_1}\left\{\left(1+f_1^e\right)\frac{\partial^2 s_1}{\partial t^2}+\frac{c_s f_1^p}{b}\frac{\partial s_1}{\partial t}-c_s^2\frac{\partial^2 v}{\partial x_1\partial t}\right\}dtd\Omega \\
&+ \int_\Omega\int_0^T \lambda_{s_2}\left\{\left(1+f_2^e\right)\frac{\partial^2 s_2}{\partial t^2}+\frac{c_s f_2^p}{b}\frac{\partial s_2}{\partial t}-c_s^2\frac{\partial^2 v}{\partial x_2\partial t}\right\}dtd\Omega \\
&+ \int_{\Gamma_{\text{free}}}\int_0^T \lambda_B\left(\frac{\partial s_2}{\partial t}-g\right)dtd\Gamma_{\text{free}} + \int_\Omega \lambda_I\frac{\partial v}{\partial t}(\mathbf{x},0)d\Omega. \qquad (12)
\end{aligned}$$

In (12), $\mathcal{L}$ consists of the misfit and the regularization term, followed by the governing PDEs, boundary, and initial conditions, the latter side-imposed by Lagrange multipliers $\lambda_v, \lambda_{s_1}, \lambda_{s_2}, \lambda_B, \lambda_I$. To alleviate the ill-posedness and thus narrow the feasibility space of the material parameter (c_s), we explore a Tikhonov regularization scheme endowed with a regularization factor (R_{c_s}) continuation algorithm that greatly aids in recovering sharp material interfaces.

3.2.1. The first optimality condition: To invert for c_s, we seek to satisfy stationarity of $\mathcal{L}$, by requiring that the first variations of $\mathcal{L}$ vanish. In particular, the variation of $\mathcal{L}$ with respect to the Lagrange multipliers $(\lambda_v, \lambda_{s_1}, \lambda_{s_2}, \lambda_B, \lambda_I)$ recovers the original state (or forward) problem, which is the same as the IBVP given by Eqs. (10b) and (11).

3.2.2. The second optimality condition: The variation with respect to the state variables (v, s_1, s_2) yields the following adjoint problem.

$$f_m\frac{\partial^2\lambda_v}{\partial t^2}-\frac{c_s}{b}f_c\frac{\partial\lambda_v}{\partial t}+\frac{c_s^2}{b^2}f_k\lambda_v-\frac{\partial}{\partial x_1}\left(c_s^2\frac{\partial\lambda_{s_1}}{\partial t}\right)-\frac{\partial}{\partial x_2}\left(c_s^2\frac{\partial\lambda_{s_2}}{\partial t}\right)=0 \text{ in } \Omega\times(0,T], \qquad (13a)$$

$$\left(1+f_1^e\right)\frac{\partial^2\lambda_{s_1}}{\partial t^2}-\frac{c_s f_1^p}{b}\frac{\partial\lambda_{s_1}}{\partial t}+c_s\frac{f_2^p}{b}\frac{\partial\lambda_v}{\partial x_1}-\left(1+f_2^e\right)\frac{\partial^2\lambda_v}{\partial x_1\partial t}=0 \text{ in } \Omega\times(0,T], \qquad (13b)$$

$$\left(1+f_2^e\right)\frac{\partial^2\lambda_{s_2}}{\partial t^2}-\frac{c_s f_2^p}{b}\frac{\partial\lambda_{s_2}}{\partial t}+c_s\frac{f_1^p}{b}\frac{\partial\lambda_v}{\partial x_2}-\left(1+f_1^e\right)\frac{\partial^2\lambda_v}{\partial x_2\partial t}=0, \text{ in } \Omega\times(0,T], \qquad (13c)$$

$$\begin{aligned}
\lambda_v(\mathbf{x},t) &= 0 && \text{on } \Gamma_{\text{fixed}}\times[0,T], && (14a)\\
c_s^2\frac{\partial\lambda_{s_2}}{\partial t}(\mathbf{x},t) &= -\sum_{j=1}^{N_r}\left[v(\mathbf{x},t)-v_m(\mathbf{x},t)\right]\delta(\mathbf{x}-\mathbf{x}_{mj}) && \text{on } \Gamma_{\text{free}}\times[0,T], && (14b)\\
\lambda_v(\mathbf{x},t) &= \dot{\lambda}_v(\mathbf{x},t)=0, && \text{in } \Omega\times\{t=T\}, && (14c)\\
\lambda_{s_1}(\mathbf{x},T) &= \dot{\lambda}_{s_1}(\mathbf{x},T)=0 && \text{in } \Omega\times\{t=T\}, && (14d)\\
\lambda_{s_2}(\mathbf{x},T) &= \dot{\lambda}_{s_2}(\mathbf{x},T)=0 && \text{in } \Omega\times\{t=T\}. && (14e)
\end{aligned}$$

Equations (13) and (14) allow a solution for λ_v, λ_{s_1}, and λ_{s_2}, once the state solution $v(\mathbf{x}, t)$ has been recovered. It is a final value problem, also endowed with PML, and can be resolved by the same mixed finite element method as the one used for the state problem.

3.2.3. The third optimality condition: Lastly, the variation with respect to the material parameter (c_s) enforces the following time-invariant control problem:

$$-R_{c_s}\Delta c_s + \int_0^T \left\{ \lambda_v \frac{f_c}{b}\frac{\partial v}{\partial t} + 2\lambda_v \frac{c_s}{b^2} f_k v + \frac{\partial \lambda_v}{\partial x_1}\frac{f_2^p}{b} s_1 + \frac{\partial \lambda_v}{\partial x_2}\frac{f_1^p}{b} s_2 \right.$$
$$\left. + \lambda_{s_1}\frac{f_1^p}{b}\frac{\partial s_1}{\partial t} - 2\lambda_{s_1} c_s \frac{\partial^2 v}{\partial x_1 \partial t} + \lambda_{s_2}\frac{f_2^p}{b}\frac{\partial s_2}{\partial t} - 2\lambda_{s_2} c_s \frac{\partial^2 v}{\partial x_2 \partial t} \right\} dt = 0. \tag{15}$$

Notice that the left-hand side of Eq.(15) implies the continuous form of the reduced gradient ($\nabla\mathcal{L}$). It is calculated based on the state and adjoint solutions previously obtained.

3.3. Inversion process

Upon discretization, the derived state, adjoint, and control problems lead to a KKT system. The KKT system can be solved for v, s_1, s_2, λ_v, λ_{s_1}, λ_{s_2}, λ_B, λ_I, and c_s using a full-space method, i.e., solving for all parameters simultaneously. However, the associated computational cost is substantial. Here, we adopt a reduced-space approach where the control variable c_s is iteratively updated using the most recent state and adjoint problem solutions. We use a conjugate gradient method with inexact line search based on the reduced gradient (15) to iteratively update the shear wave velocity profile.

4. Numerical Examples

We consider first a one-dimensional wave velocity profile of semi-infinite soil medium as depicted in Fig. 3, where, for simplicity, the physical quantities are chosen as dimensionless. The PML occupies $1.0 < x < 1.2$. We attempt to reconstruct this target profile within the regular domain ($0 < x < 1$) by applying a Gaussian-type pulse load with frequency range between 0 and 40Hz. Figure 4 shows the reconstructed wave velocity profiles (red dots) of the layered soil medium using Total Variation (TV) and Tikhonov (TN) regularization schemes. The inversion process started from an initial guess (green dots) of 0.86 with a fixed regularization factor $R_c = 10^{-6}$. Both schemes recovered the true profile fairly well. We remark that the TV regularization scheme captures the sharply varying profile better than TN scheme when the regularization factor (R_c) is not allowed to vary. Next, we look into the inversion of a shear wave velocity profile in two

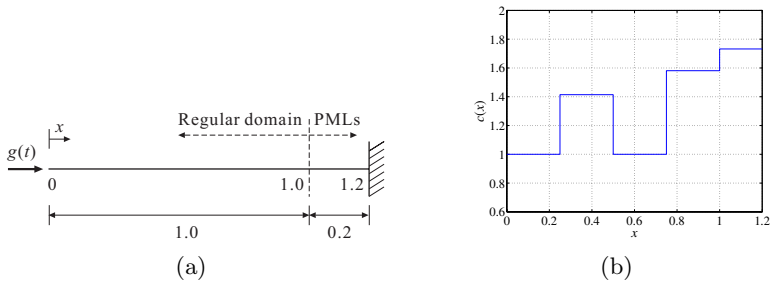

(a) (b)

Figure 3. (a) Configuration of the one-dimensional PML-truncated semi-infinite domain (b) Target wave velocity profile $c(x)$

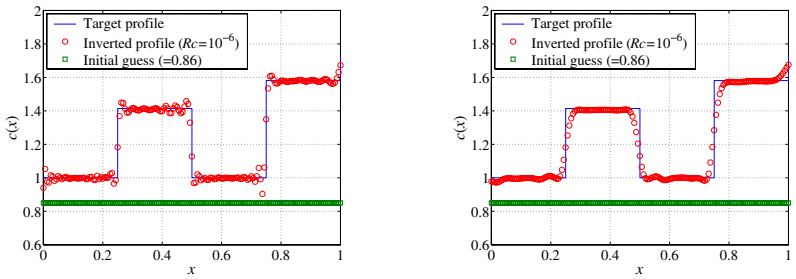

Figure 4. Initial guess, target, and inverted wave velocity profile using (a) TV regularization (b) TN regularization

dimensions. The problem configuration is shown in Fig. 1b. A distributed Ricker pulse load $\sigma_{32} = g(t)$ is imposed on the surface of the regular domain and 101 receivers measure the surficial displacement responses. In Fig. 5, a layered shear wave velocity profile with $c_s = 2.0, 2.3, 1.6,$ and 2.6km/s from top to bottom is successfully reconstructed. In Fig. 6, the profile with 5 layers has an elliptical inclusion with $c_s = 2.8$km/s. The layers in this case have velocities of $c_s = 2.0, 2.2, 2.4, 2.6,$ and 2.8km/s, respectively. Figure 6 shows that the inclusion is detected quite well, exposing the value of c_s as well as its location and shape. In Fig. 7, the layers are curved with the same c_s distribution as in Fig. 6. We see that the curved profiles are recovered reasonably well. For all these examples, a regularization factor continuation algorithm was used with a starting factor of $R_{c_s} = 10^{-5}$.

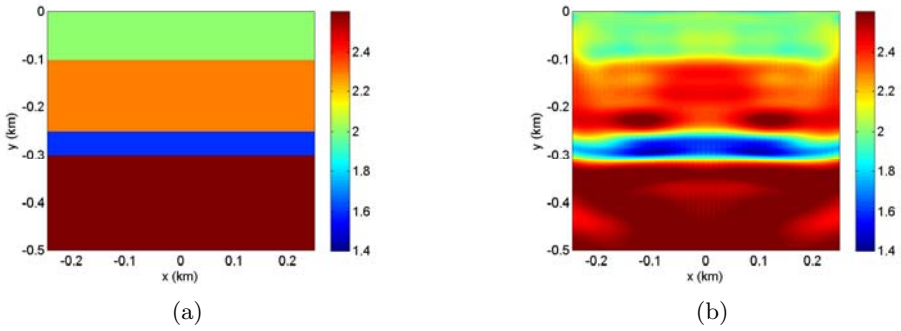

Figure 5. (a) A 2D target shear wave velocity profile with 4 layers (c_s = 2.0km/s, 2.3km/s, 1.6km/s, and 2.6km/s from top to bottom) (b) Reconstructed profile

5. Conclusions

We discussed a PDE-constrained optimization approach for treating directly in the time-domain the inverse medium problem that arises in semi-infinite domains illuminated by surface excitation sources. To alleviate solution multiplicity we used Tikhonov regularization endowed with a continuation scheme on the regularization parameter to speed convergence. To date, the numerical experiments have shown satisfactory performance in reconstructing heterogeneous material profiles. The methodology is systematic and scales naturally to the more challenging three-dimensional elasticity case.

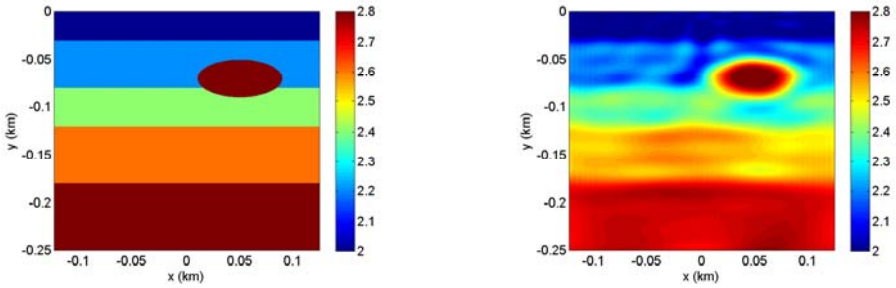

(a) (b)

Figure 6. A 2D target shear wave velocity profile with 5 layers and inclusion (Layer: c_s = 2.0km/s, 2.2km/s, 2.4km/s, 2.6km/s, and 2.8km/s from top to bottom, Inclusion: c_s = 2.8km/s) (b) Reconstructed profile

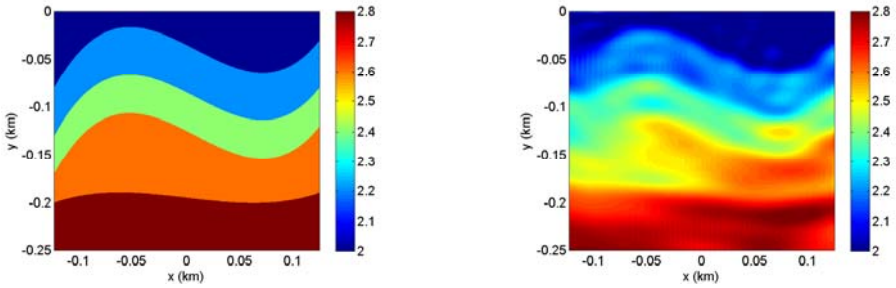

(a) (b)

Figure 7. A 2D target shear wave velocity profile with 5 curved layers (Layer: c_s = 2.0km/s, 2.2km/s, 2.4km/s, 2.6km/s, and 2.8km/s from top to bottom) (b) Reconstructed profile

Acknowledgment

Partial support for the authors' research has been provided by the National Science Foundation under grant awards CMS-0348484 and ATM-0325125. This support is gratefully acknowledged.

References

[1] Kallivokas L F and Lee S 2004 Local absorbing boundaries of elliptical shape for scalar waves *Comput. Method Appl. M.* **193** (45-47) 4979-5015

[2] Givoli D and Keller J B 1990 Non-reflecting boundary conditions for elastic waves *Wave Motion* **12** (3) 261-279

[3] Basu U and Chopra A K 2003 Perfectly matched layers for time-harmonic elasto-dynamics of unbounded domains : theory and finite-element implementation *Comput. Method Appl. M.* **192** 1337-75

[4] Basu U and Chopra A K 2004 Perfectly matched layers for transient elastodynamics of unbounded domains *Int. J. Numer. Meth. Eng.* **59** 1039-74

[5] Collino F and Tsogka C 2001 Application of the perfectly matched absorbing layer model to the linear elastodynamic problem in anisotropic heterogeneous media *Geophysics*, **66** (1) 294–307

[6] Carey G F and Oden J T 1983 *Finite elements - A second course* Vol II (Prentice Hall)

[7] Akcelik V 2002 *Multiscale Newton-Krylov methods for inverse acoustic wave propagation: Doctoral dissertation* (Carnegie Mellon University, Pittsburgh, PA, USA)

[8] Biros G and Ghattas O 1999 *Parallel Newton-Krylov Methods for PDE-constrained optimization: Proceedings of Supercomputing* (Portland, Oregon, USA)